Supporting Information for "*Relevant electronic interactions related to the coordination chemistry of tetracyanometallates. An XPS study*, by Cano, I. Monroy, M. Ávila, D. Velasco-Arias, J. Rodríguez-Hernández, E. Reguera
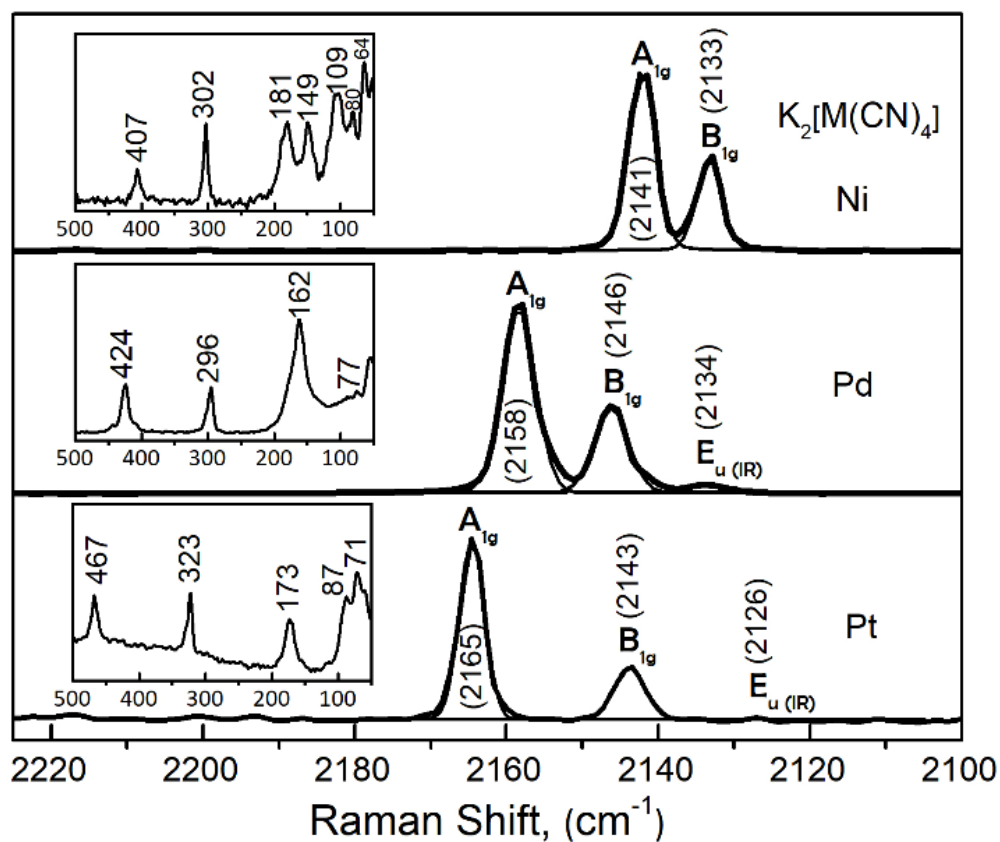


Figure S1: Raman spectra for $K_2[M(CN)_4]$ where M= Ni, Pd and Pt.  In the $\nu$(CN) spectral region the CN stretching $A_{1g}$ and $B_{1g}$ vibrations are observed, which are Raman active,  and also the $E_u$ IR active mode, which appears as a weak absorption band. Inset: Low frequency spectral region. Table S1 summarizes the assignment of the observed vibrations in the Raman spectra.

Table S1: Assignment of the observed vibrations in the Raman spectra for $K_2[M(CN)_4]$ where M= Ni, Pd and Pt.

| Vibrational mode | $K_2[Ni(CN)_4]$ | $K_2[Pd(CN)_4]$ | $K_2[Pt(CN)_4]$ |
|---|---|---|---|
| $A_{1g}$, $\nu(C\equiv N)$ | 2141 | 2158 | 2165 |
| $B_{1g}$, $\nu(C\equiv N)$ | 2133 | 2146, 2134 ($E_u$) | 2143, 2126 ($E_u$) |
| $A_{1g}$, $\nu(M-C)$ | 407 | 424 | 467 |
| $E_g$, $\pi(M-C-N)$ | 302 | 296 | 323 |
| $B_{2g}$, $\delta(M-C-N)$ | 181 | 162 | 171 |
| $E_u$, $\delta(C-M-C)$ | 109 | - | - |
| $A_{2u}$, $\omega(C-M-C)$ | 80 | 77 | 87 |
| $B_{2u}$, $\tau(C-M-C)$ | 64 | - | 71 |

This assignment was made according to the information available in: 1) K. Nakamoto (2009): Infrared and Raman Spectra of Inorganic and Coordination Compounds, Part B: Applications in Coordination, Organometallic, and Bioinorganic Chemistry, Hoboken, New Jersey; 2) D. Jones, I. J. Hyams, E. R. Lippincott, Laser Raman spectrum and vibrational assignment of the tetracyanonickellate ion, *Spectrochimica Acta Part A.* 1968, **24**, 973-980.

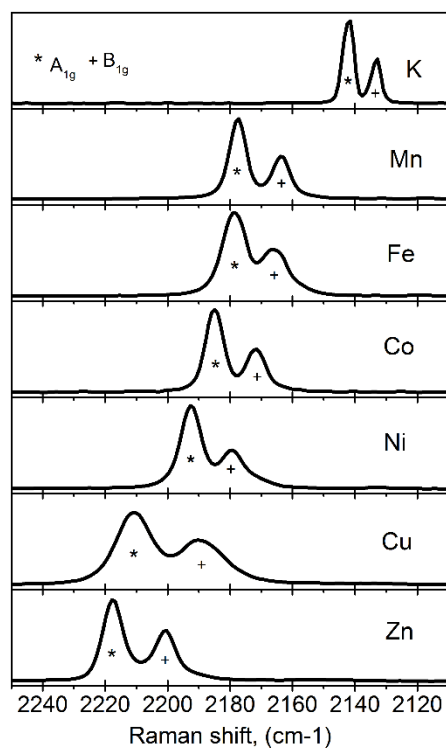

Figure S2. $\nu(CN)$ stretching region for the Raman spectra of $K_2[Ni(CN)_4]$ and $T[M(CN)_4]\cdot XH_2O$ series where T= Mn, Fe, Co, Ni, Cu and Zn. Table S2 contains the frequency values.

Table S2. The Raman active vibrational modes (in cm$^{-1}$) for the T[M(CN)$_4$]·XH$_2$O series where T= Mn, Fe, Co, Ni, Cu and Zn.

| Vibrational mode | Mn | Fe | Co | Ni | Cu | Zn |
|---|---|---|---|---|---|---|
| A$_{1g}$, ν(C≡N) | 2177 | 2178 | 2207 | 2215 | 2211 | 2217 |
| B$_{1g}$, ν(C≡N) | 2163 | 2166 | 2151 | 2149 | 2189 | 2200 |
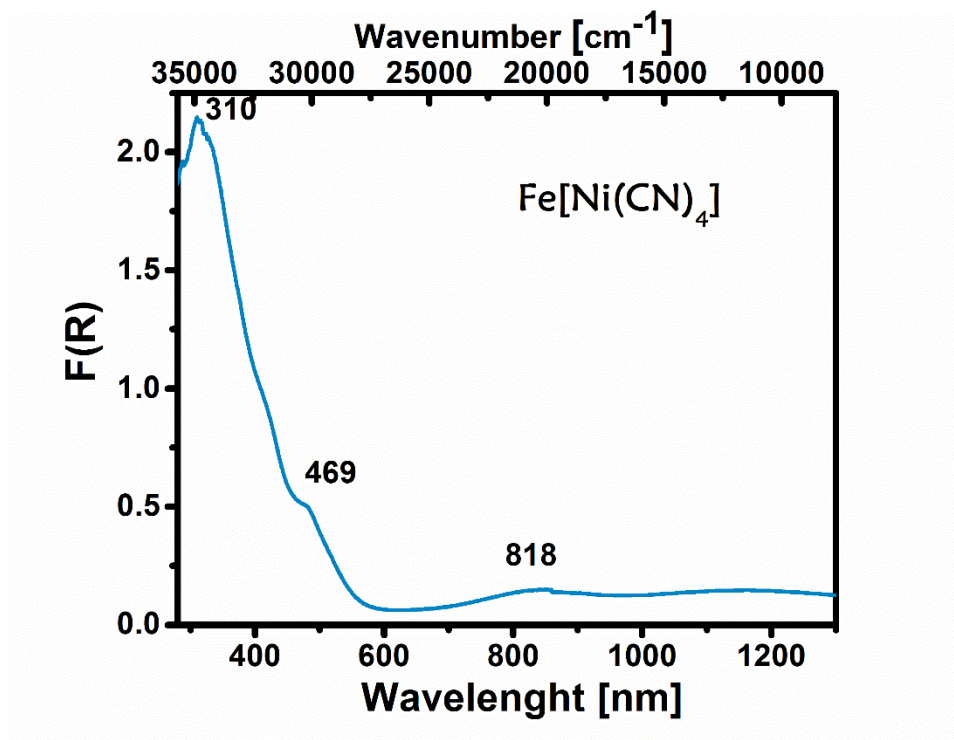


Figure S3: UV-vis spectrum for Fe[Ni(CN)$_4$]·xH$_2$O
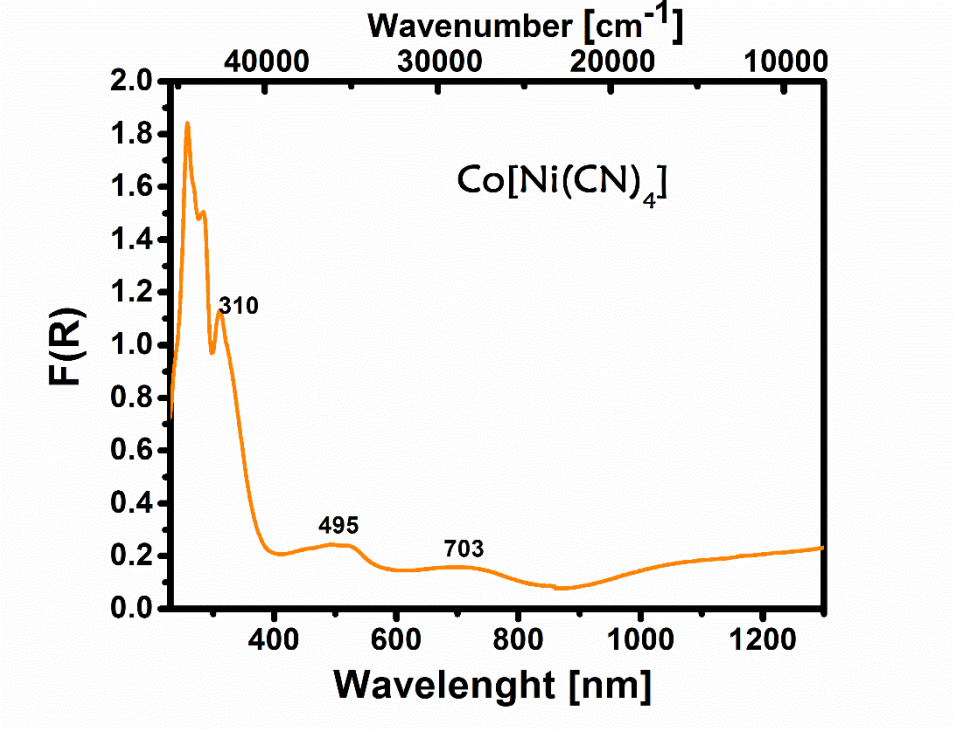
Figure S4: UV-vis spectrum for Co[Ni(CN)$_4$]·xH$_2$O
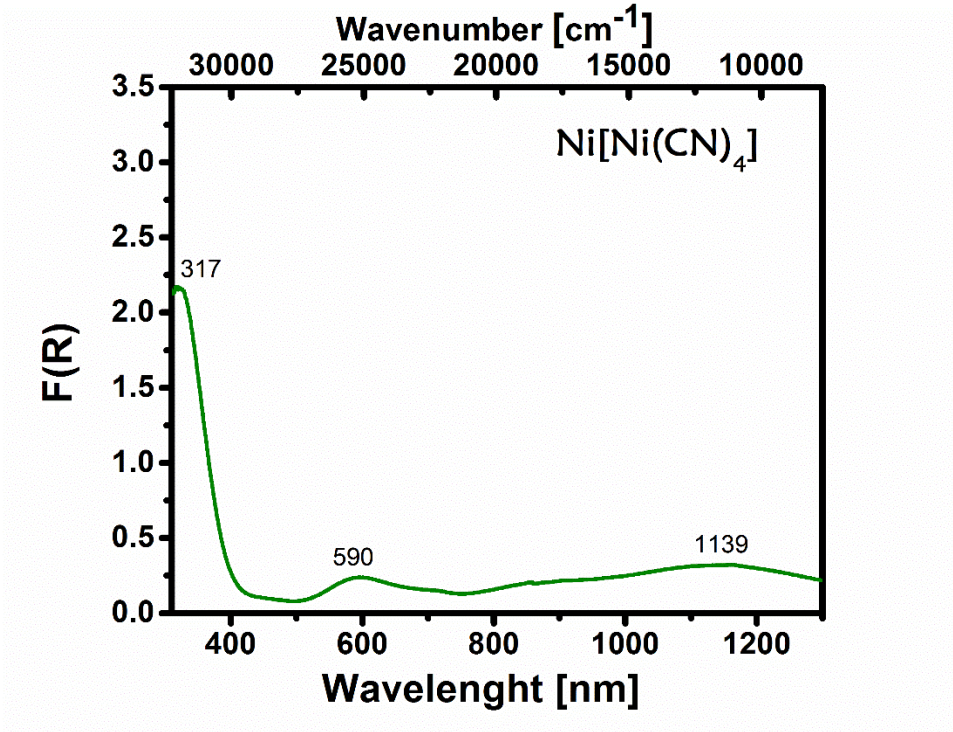


Figure S5: UV-vis spectrum for Ni[Ni(CN)$_4$]·xH$_2$O
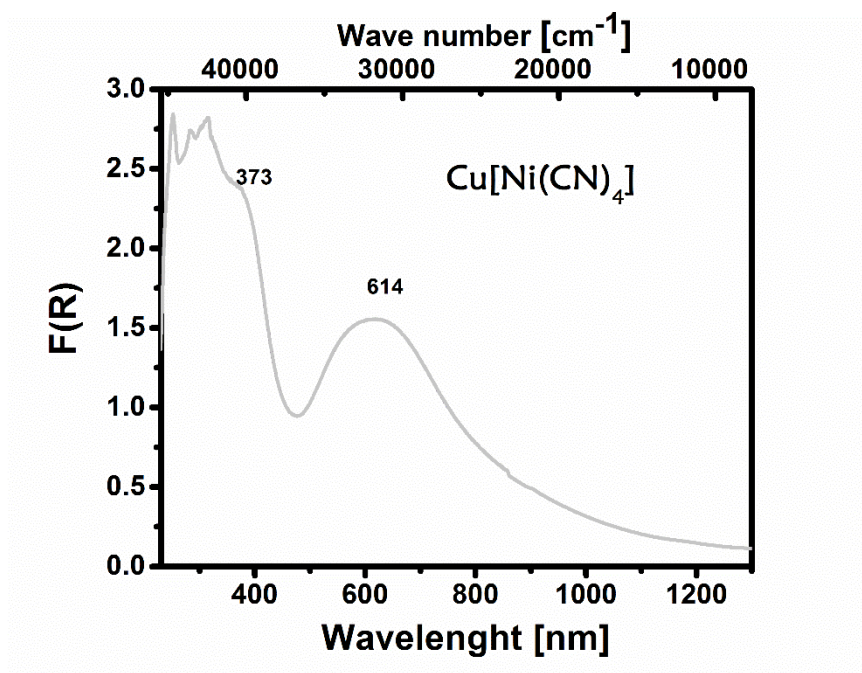
Figure S6: UV-vis spectrum for Cu[Ni(CN)$_4$]·xH$_2$O
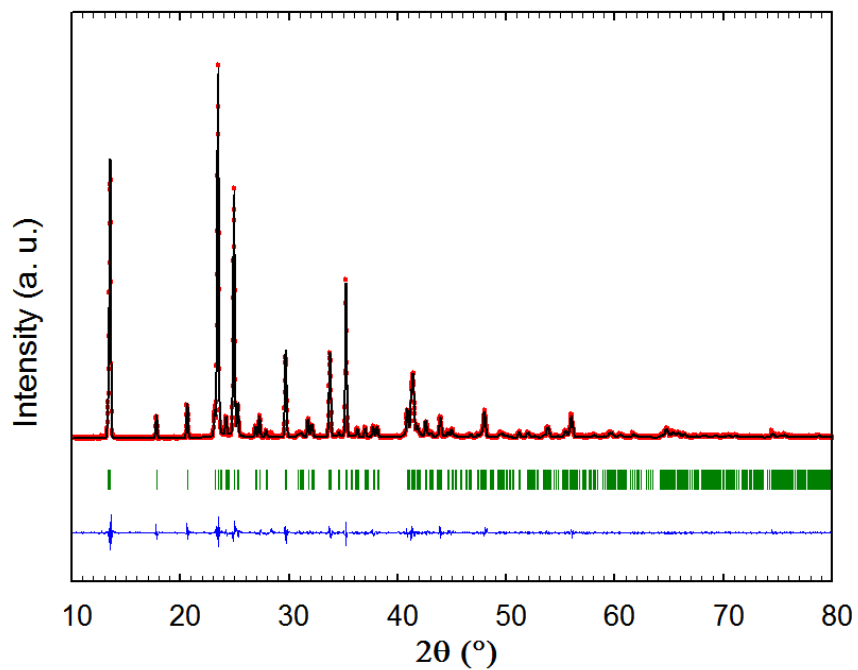


Figure S7. XRD powder pattern observed (red), calculated (black) and difference profiles (blue) for the Le Bail refinement of K$_2$[Ni(CN)$_4$] complex. The crystalline phase was identified according to ICSD file number 24099.
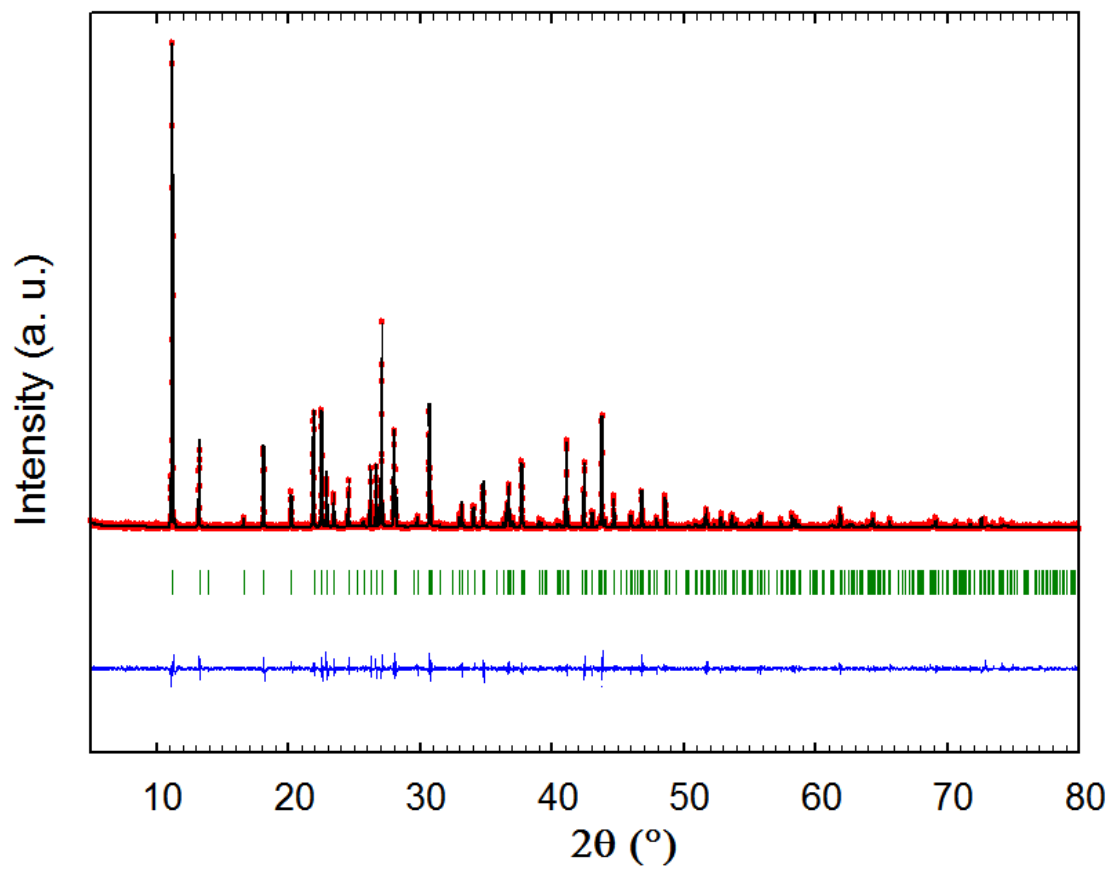
Figure S8. XRD powder pattern observed (red), calculated (black) and difference profiles (blue) for the Le Bail refinement of $K_2[Pd(CN)_4] \cdot XH_2O$ complex. The crystalline phase was identified according to ICSD file number 413900.
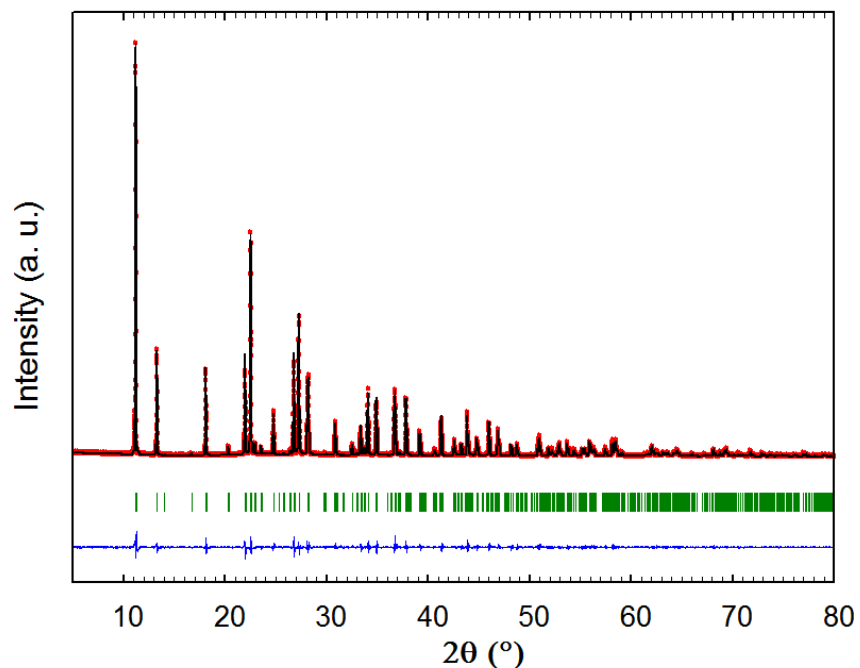
Figure S9. XRD powder pattern observed (red), calculated (black) and difference profiles (blue) for the Le Bail refinement of $K_2[Pt(CN)_4] \cdot XH_2O$ complex. The crystalline phase was identified according to ICSD file number 413901.
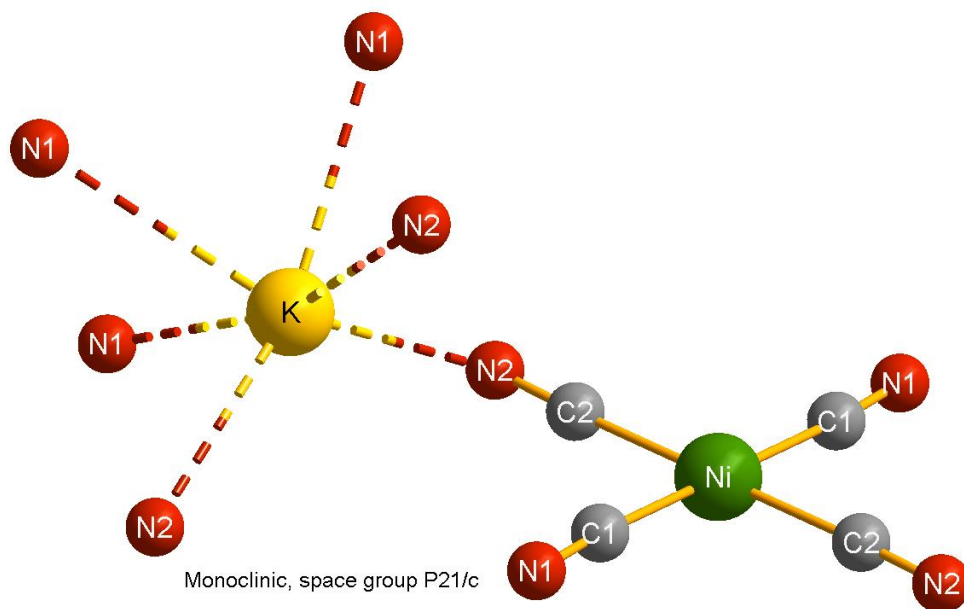


Monoclinic, space group P21/c

Figure S10: Coordination environments for K in $K_2[Ni(CN)_4]$. This potassium salt crystallizes with a monoclinic unit cell in the $P2_1/c$ space group. One structural site is available for K atom, with a coordination sphere $K(N_{CN})_6$.
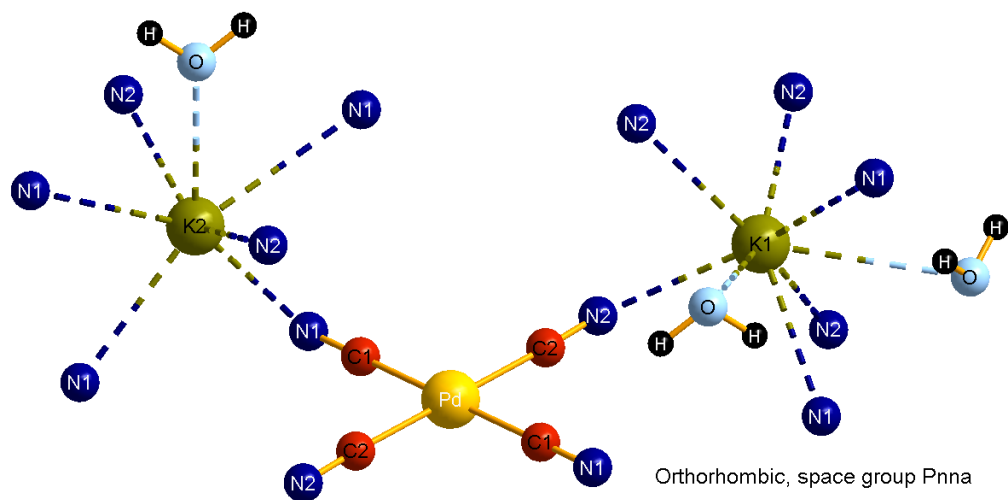
Figure S11: Coordination environments for K in $K_2[Pd(CN)_4]\cdot xH_2O$. This potassium salt crystallizes with an orthorhombic unit cell in the Pnna space group. Two structural sites are available for K atom, with a mixed coordination sphere $K(N_{CN})_6(H_2O)_2$ and $K(N_{CN})_6(H_2O)$.
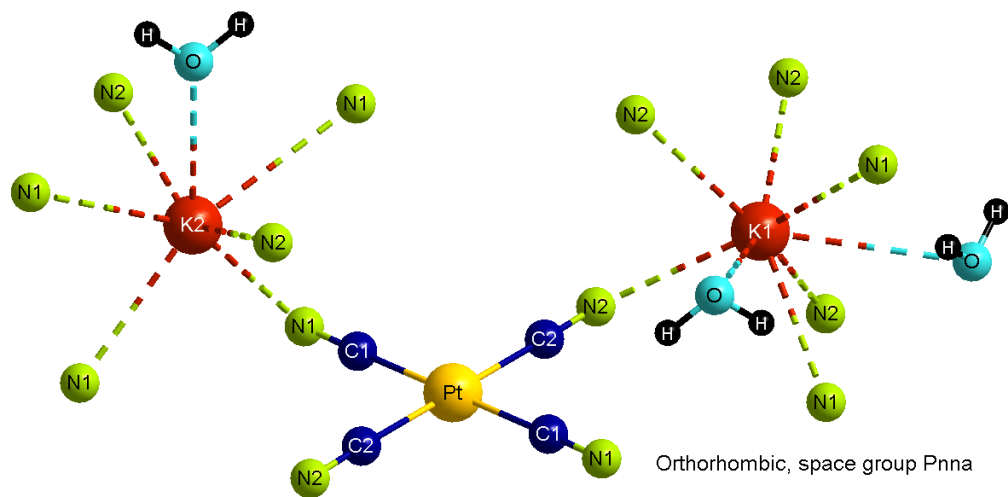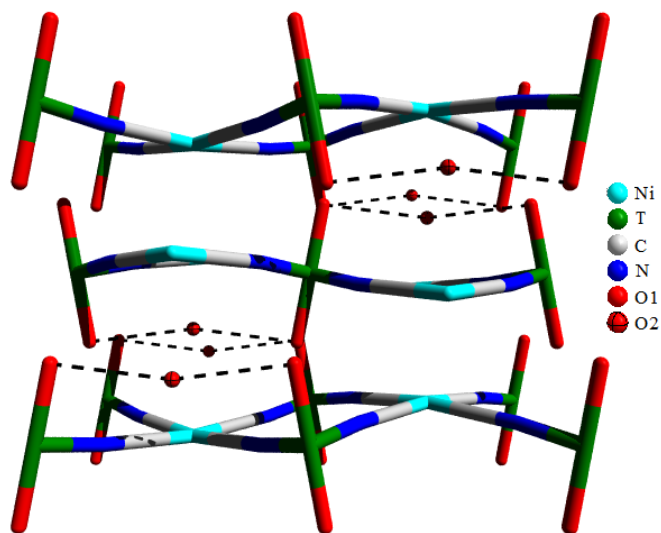


Figure S12: Coordination environments for K in $K_2[Pt(CN)_4]\cdot xH_2O$. This potassium salt crystallizes with an orthorhombic unit cell in the Pnna space group. Two structural sites are available for K atom, with a mixed coordination sphere $K(N_{CN})_6(H_2O)_2$ and $K(N_{CN})_6(H_2O)$.

Figure S13: Illustrative 3D framework for $L_1$ phase in divalent 3d metal tetracyanonickellates, $T(H_2O)_2[Ni(CN)_4] \cdot 1H_2O$. The system of stacked layers forms an ordered 3D structure through a network of hydrogen bonding.
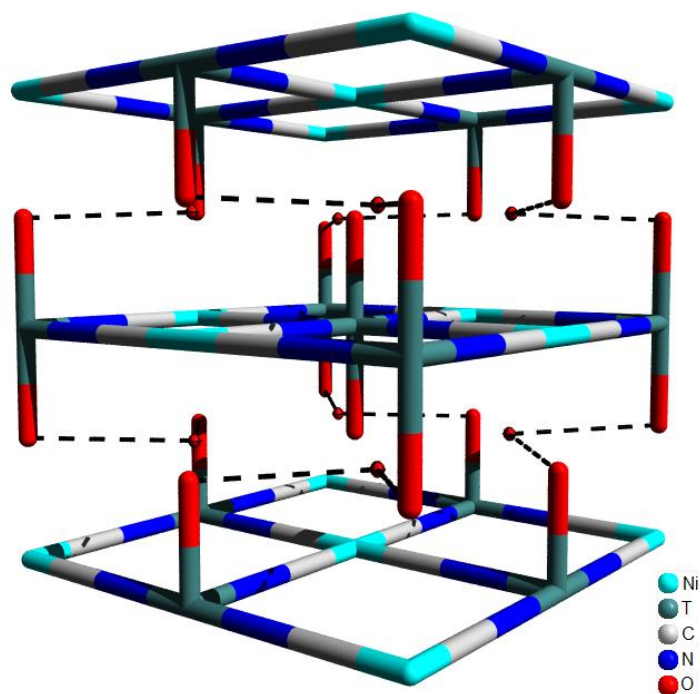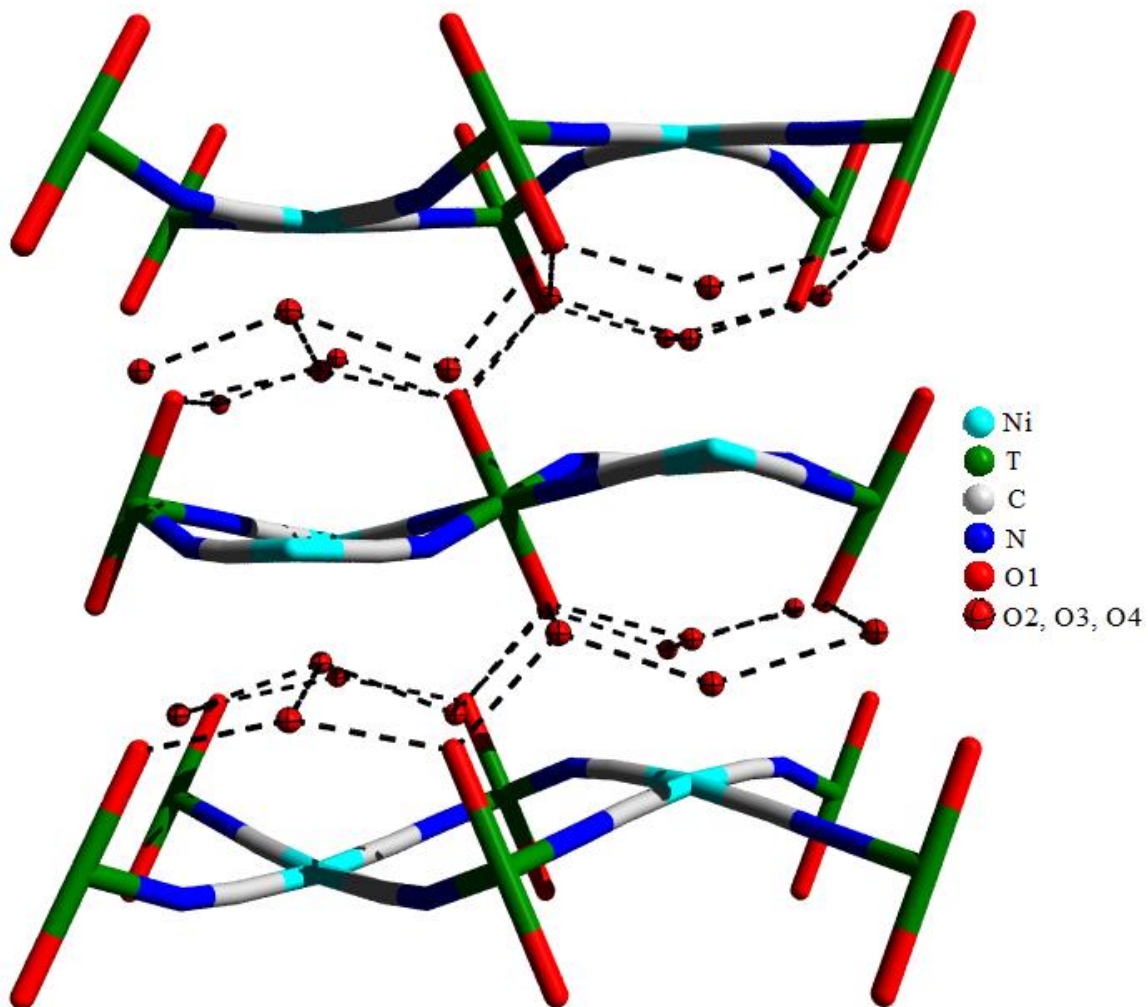


Figure S14: Illustrative 3D framework for K phase in divalent 3d metal tetracyanonickellates, $T(H_2O)_2[Ni(CN)_4] \cdot 2H_2O$. The system of stacked layers forms an ordered 3D structure through a network of hydrogen bonding.
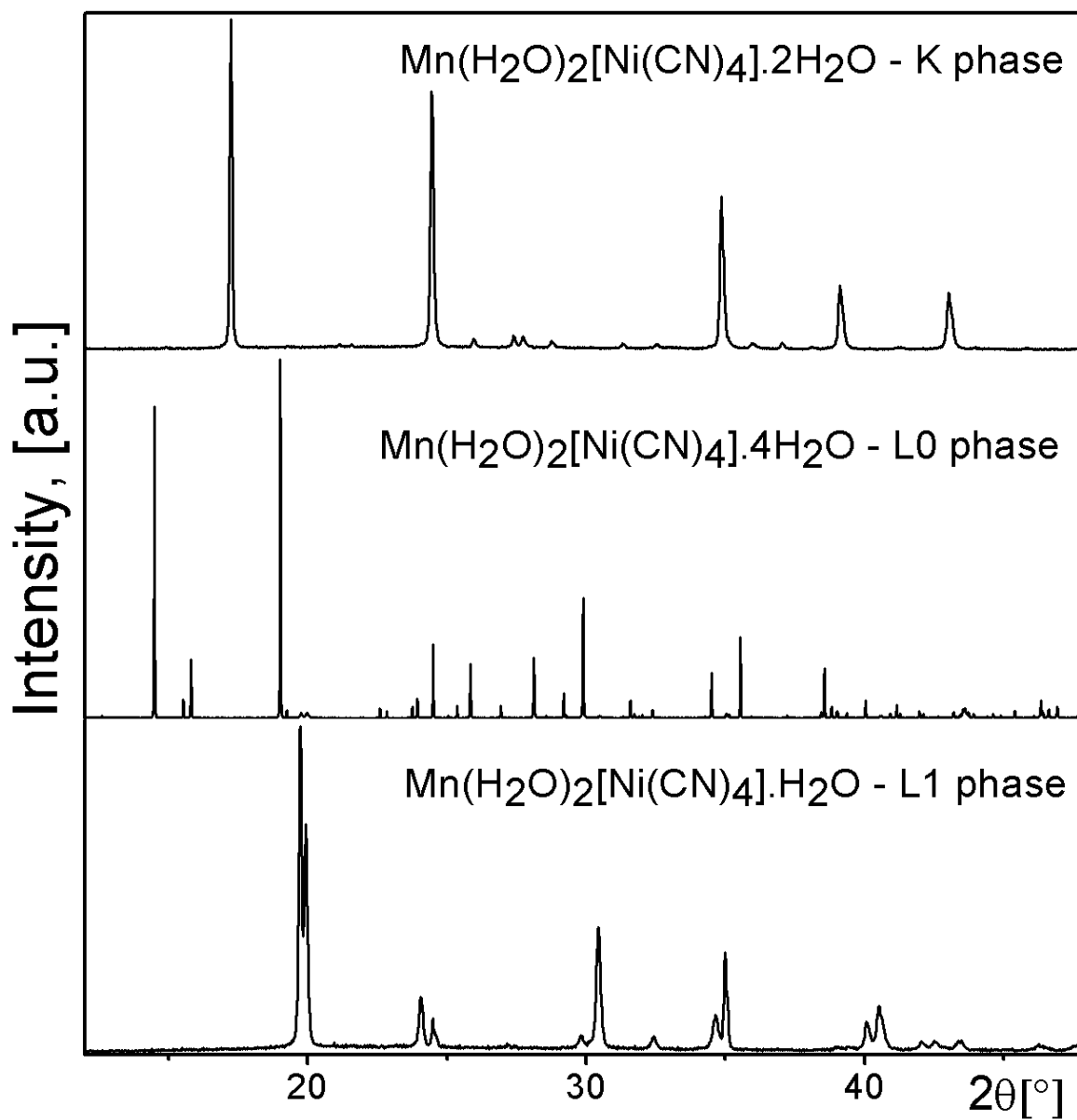
Figure S15: Illustrative 3D framework for $L_0$ phase in divalent 3d metal tetracyanonickellates, $T(H_2O)_2[Ni(CN)_4]\cdot 4H_2O$. The system of stacked layers forms an ordered 3D structure through a network of hydrogen bonding.

Figure S16: XRD powder pattern for $Mn(H_2O)_2[Ni(CN)_4] \cdot xH_2O$, illustrating the formation of three crystalline phases ($L_0$, K, and $L_1$).
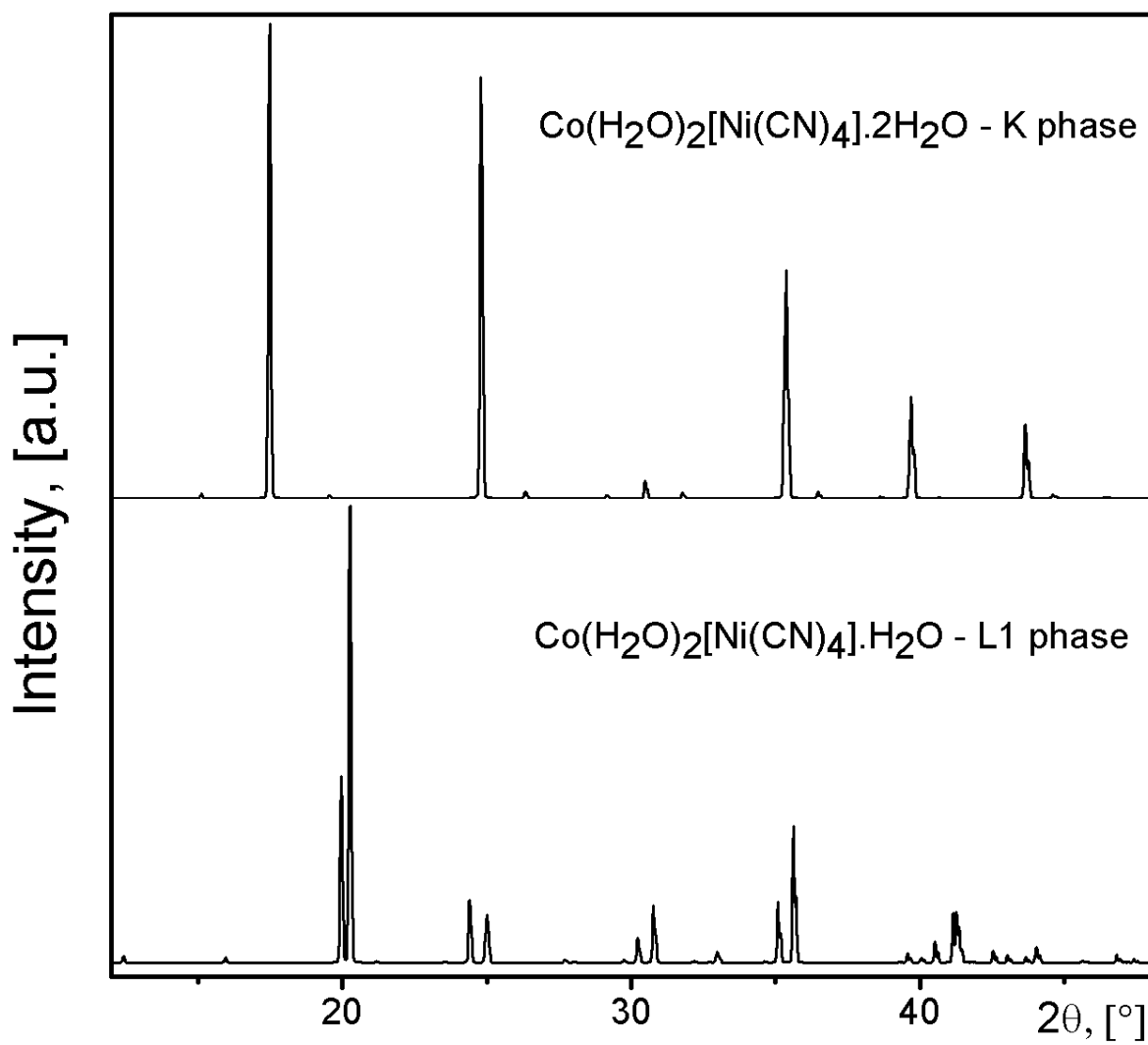
Figure S17: XRD powder pattern for $Co(H_2O)_2[Ni(CN)_4]\cdot xH_2O$, illustrating the formation of two crystalline phases (K and $L_1$).
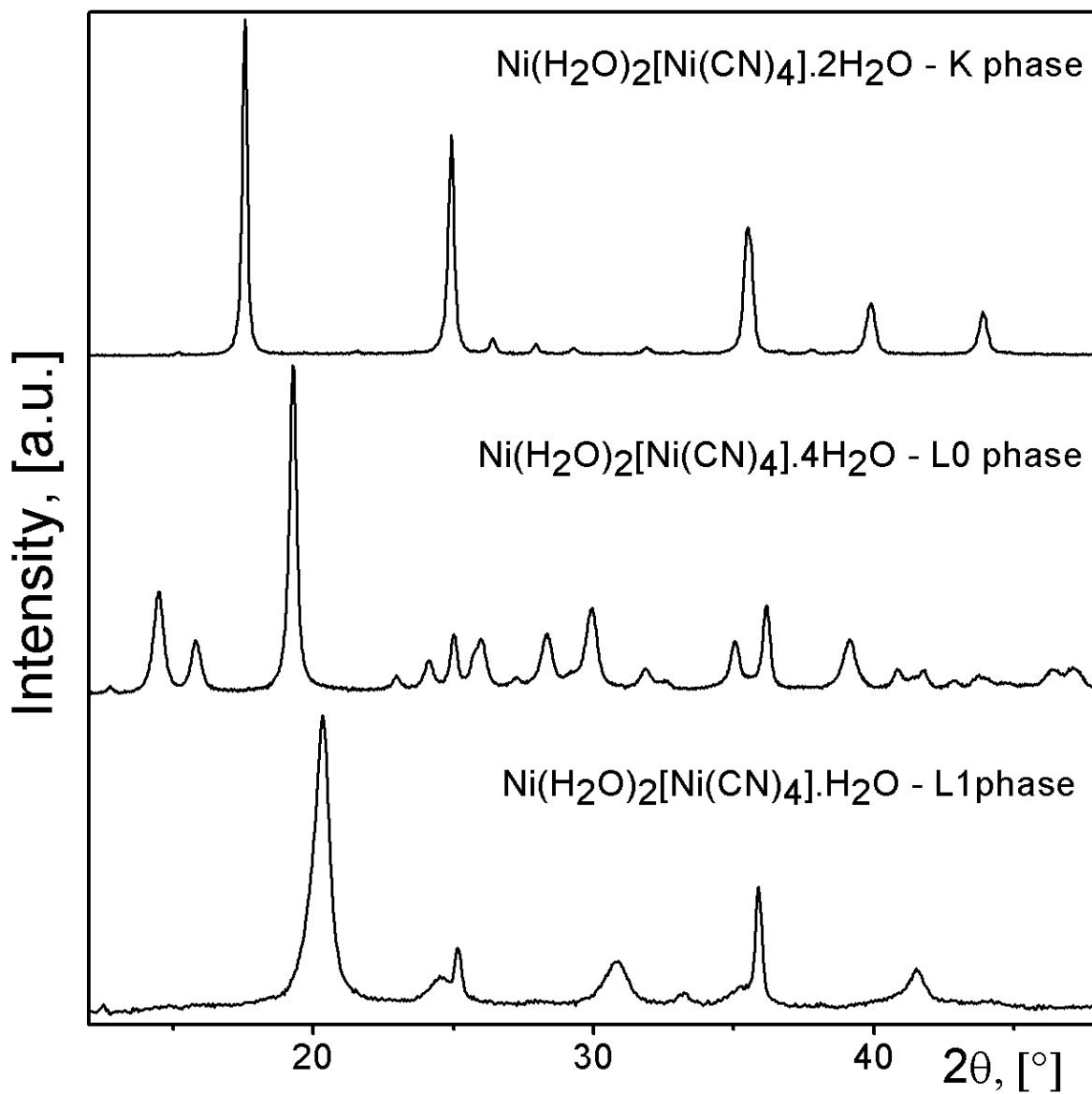
Figure S18: XRD powder pattern for $Ni(H_2O)_2[Ni(CN)_4] \cdot xH_2O$, illustrating the formation of three crystalline phases ($L_0$, K, and $L_1$).
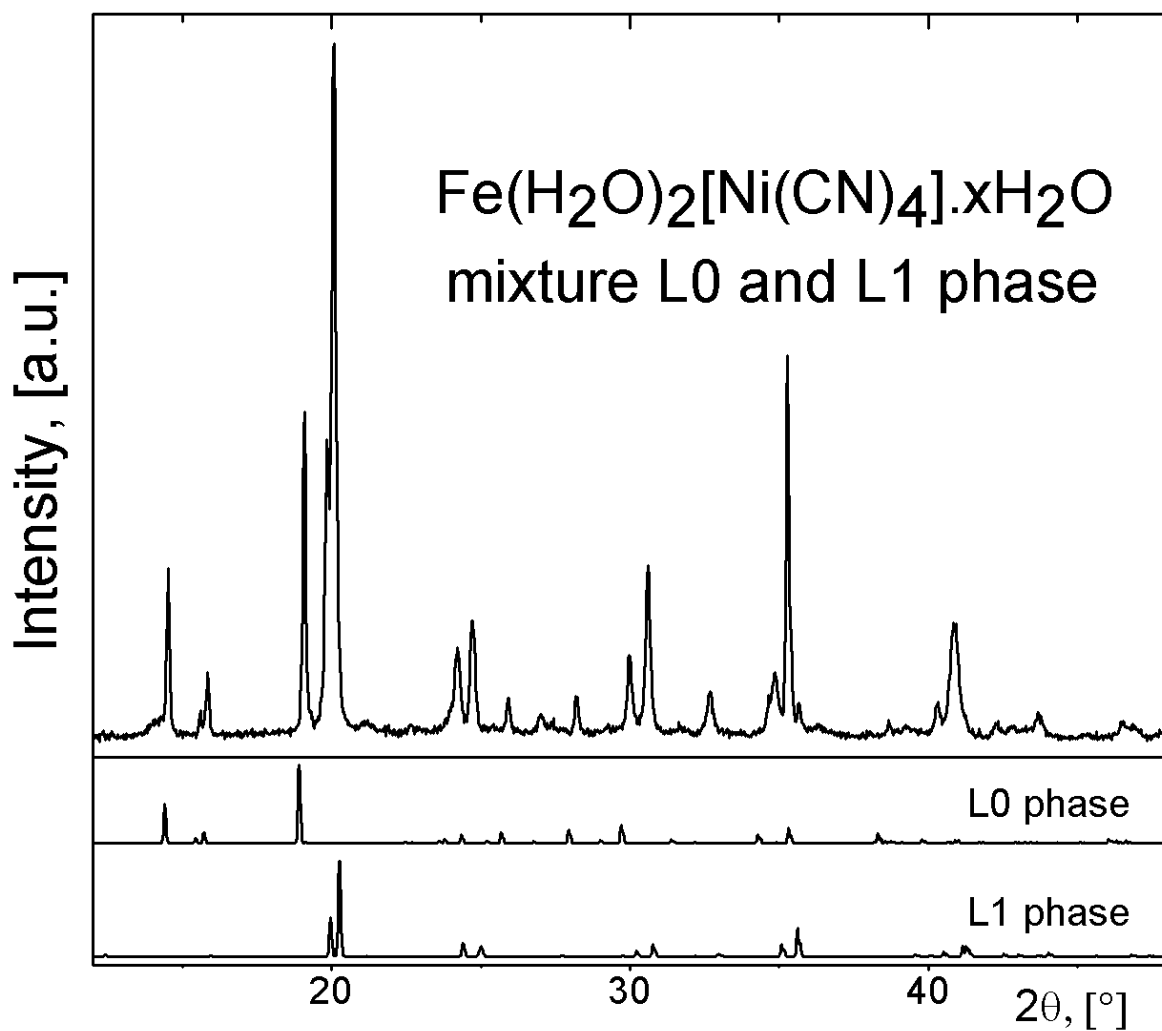
Figure S19: XRD powder patterns for $Fe(H_2O)_2[Ni(CN)_4]\cdot xH_2O$, illustrating the formation of two phases.
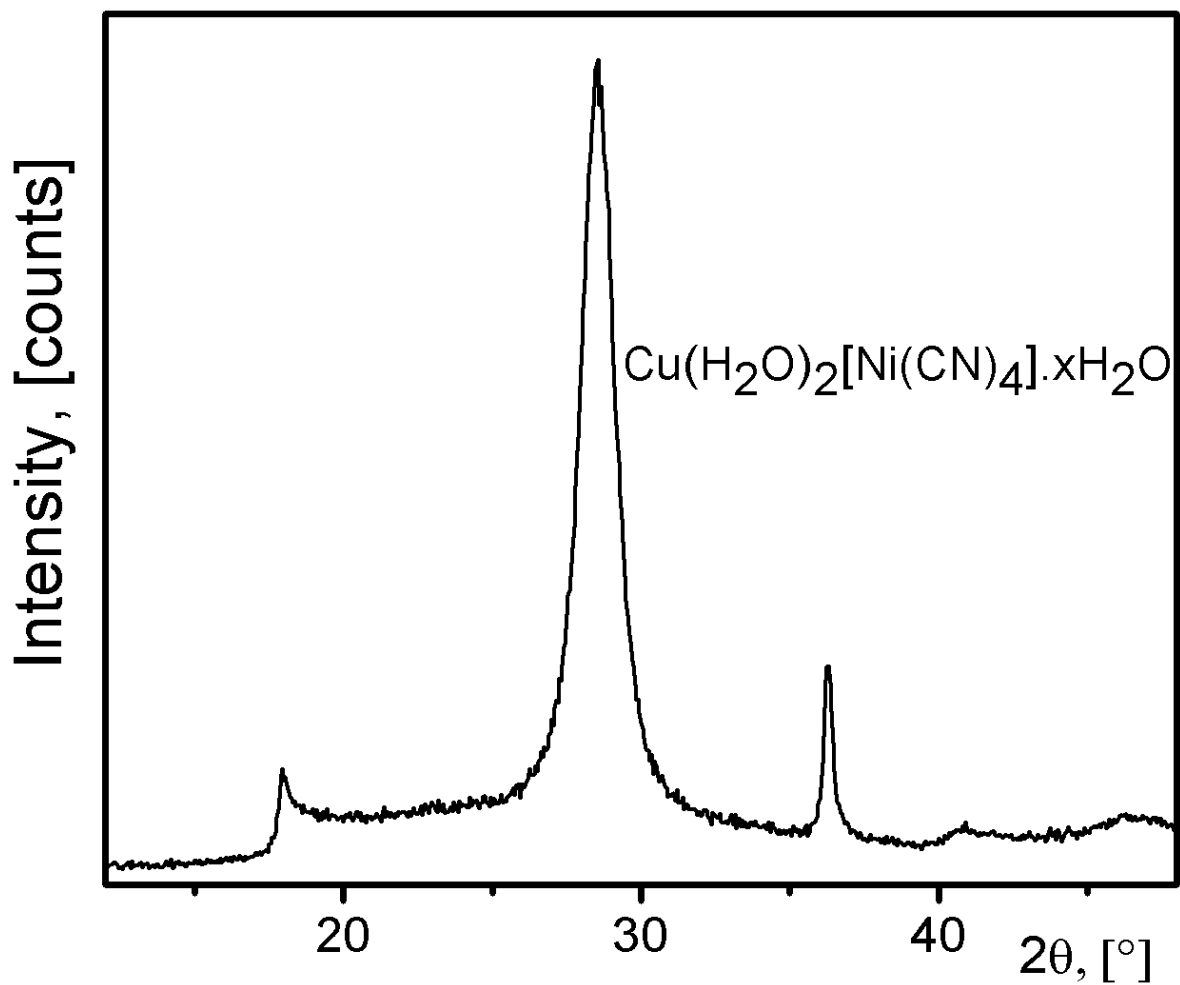
Figure S20: XRD powder pattern for $Cu(H_2O)_2[Ni(CN)_4]\cdot xH_2O$, illustrating the formation of a phase of low crystallinity.
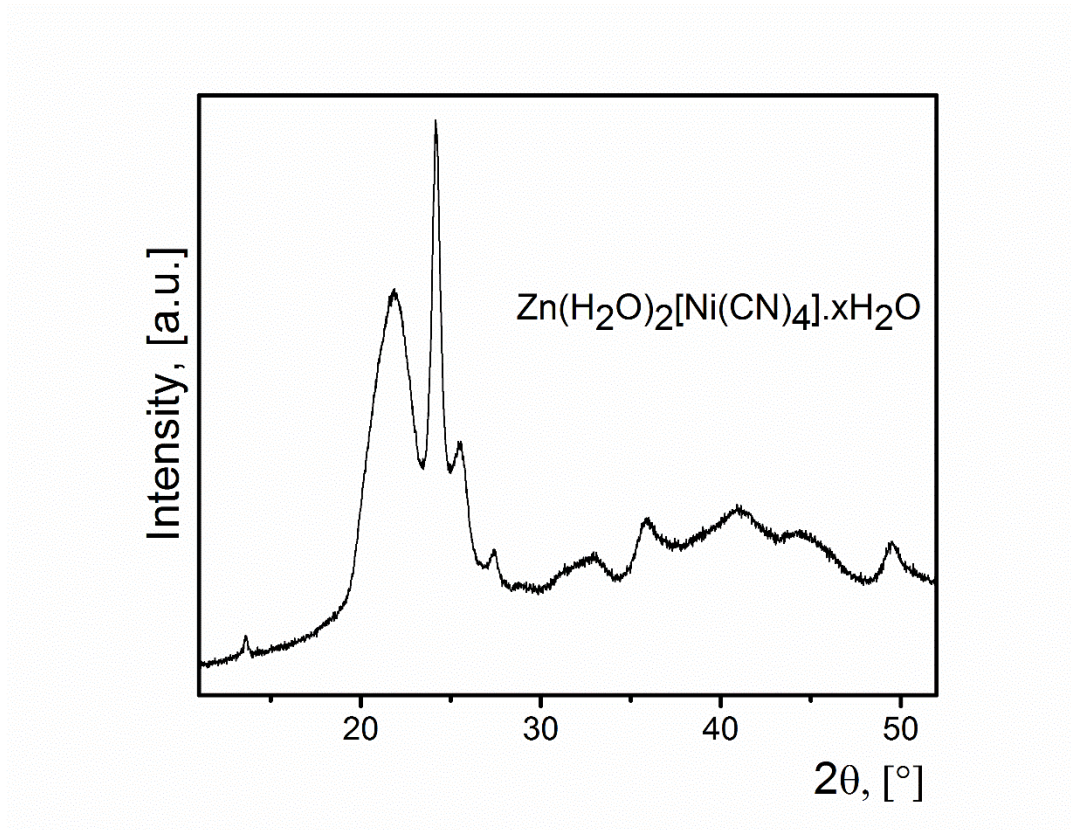
Figure S21: XRD powder pattern for Zn(H$_2$O)$_2$[Ni(CN)$_4$]·xH$_2$O, illustrating the formation of a phase of low crystallinity.
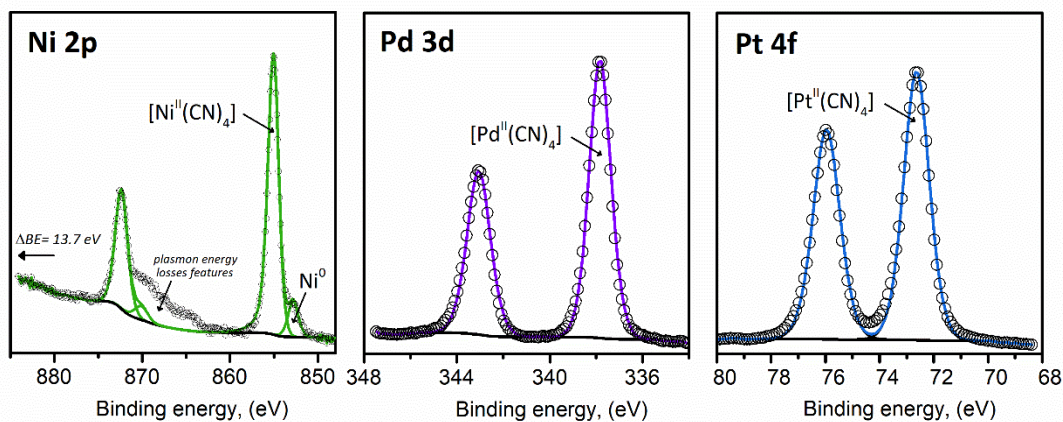


Figure S22: Metal (M) core-levels spectra for K$_2$[M(CN)$_4$] where M= Ni, Pd and Pt. Ni 2p spectrum shown additional contributions at higher energy side of Ni 2p$_{3/2}$ (≈13 eV), that can be assigned to plasmon energy losses features and the inaccurate background removal Shirley-type.
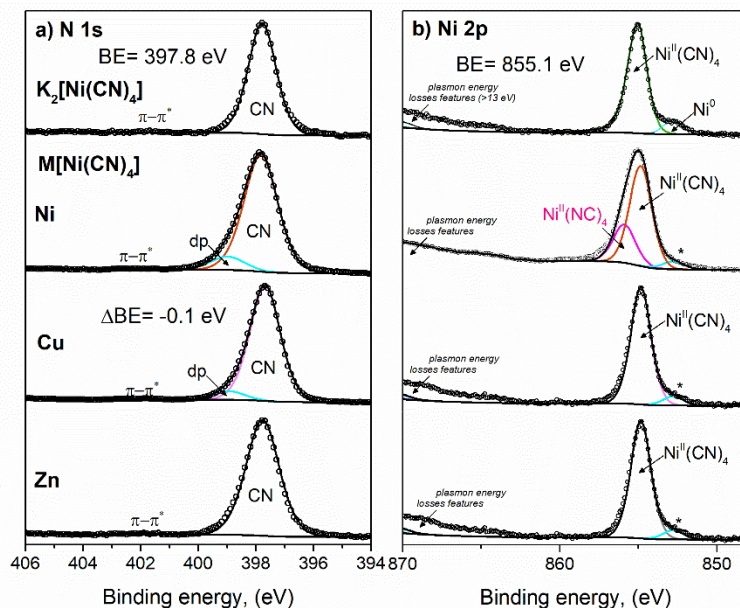
Figure S23. XPS curve-fitting results from N 1s and Ni 2p spectra from $K_2[Ni(CN)_4]$ and the $T[Ni(CN)_4] \cdot xH_2O$ series where T= Ni, Cu and Zn.
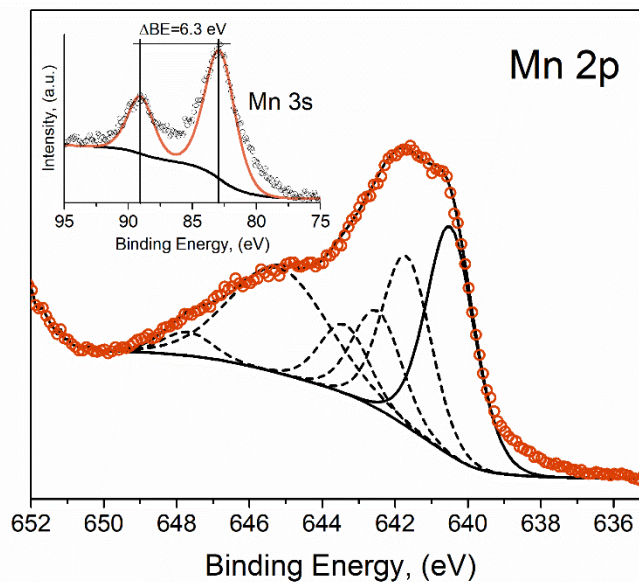


Figure S24: Mn 2p core-level spectra fitted according to the multiplet model for $Mn(H_2O)_2[Ni(CN)_4] \cdot xH_2O$. Inset: Mn 3s spectrum. XPS Curve-fitting following the model applied at Grosvenor, A. P., Biesinger, M. C., Smart, R. St. C. and McIntyre, S. N. (2006), New interpretations of XPS spectra of nickel metal and oxides. *Surf. Sci.*, 600: 1771-1779. doi: 10.1016/j.susc.2006.01.041
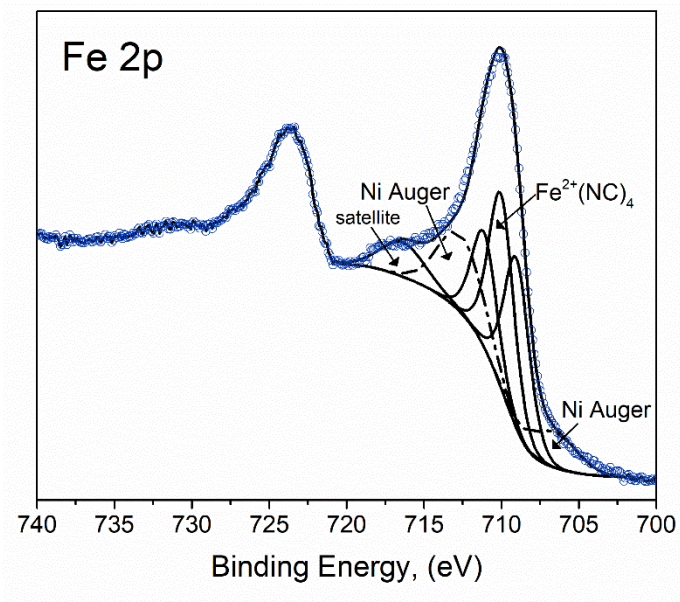
Figure S25: Fe $2p_{3/2}$ core-level peak for Fe(H$_2$O)$_2$[Ni(CN)$_4$]·xH$_2$O with its satellites. In this region also the Ni Auger peaks appear. XPS Curve-fitting following the model applied at Grosvenor, A. P., Kobe, B. A., Biesinger, M. C. and McIntyre, N. S. (2004), Investigation of multiplet splitting of Fe 2p XPS spectra and bonding in iron compounds. *Surf. Interface Anal.*, 36: 1564-1574. doi:10.1002/sia.1984
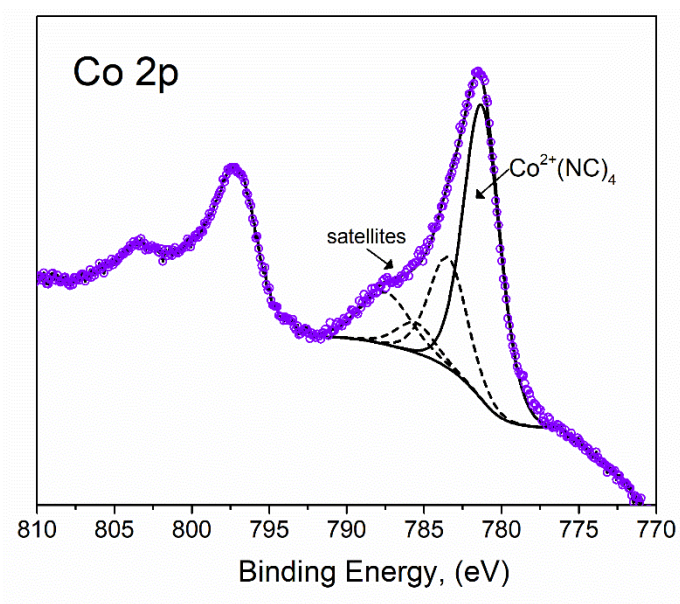


Figure S26: Co 2p core-level spectrum for Co(H$_2$O)$_2$[Ni(CN)$_4$]·xH$_2$O. The main peaks (Co $2p_{3/2}$ and Co $2p_{1/2}$) are accompanied of their respective satellites.  About 775 eV the Co LMM Auger spectrum is observed. Curve-fitting following the model applied by Biesinger, B. P., Payne, B. P., Grosvenor, A. P., Lau, L. W. M., Gerson, A. R., Smart, R. St. C., in *Applied Surface Science*, (2011) 257: 2717-2730.
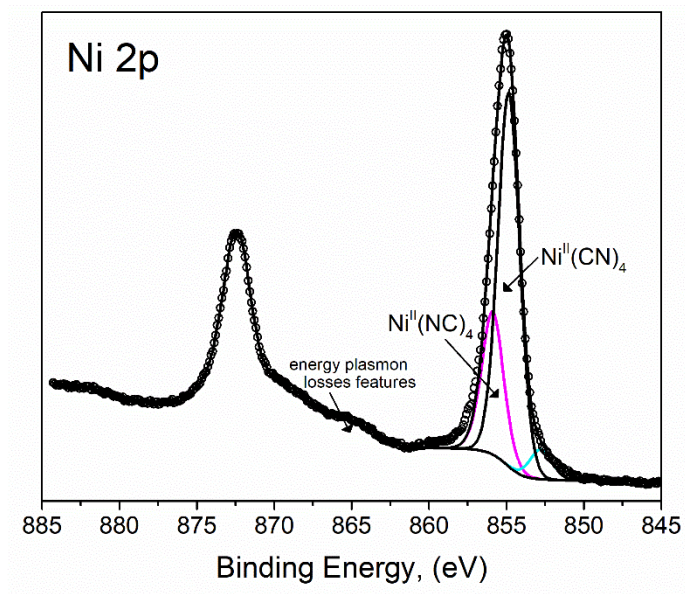
Figure S27: Ni 2p core-level peak for $Ni(H_2O)_2[Ni(CN)_4] \cdot xH_2O$. In this region the formation of a $Ni^0$ species due to the sample damage during the XPS experiment is detected. XPS Curve-fitting following the model applied at Grosvenor, A. P., Biesinger, M. C., Smart, R. St. C. and McIntyre, S. N. (2006), New interpretations of XPS spectra of nickel metal and oxides. Surf. Sci., 600: 1771-1779. doi: 10.1016/j.susc.2006.01.041
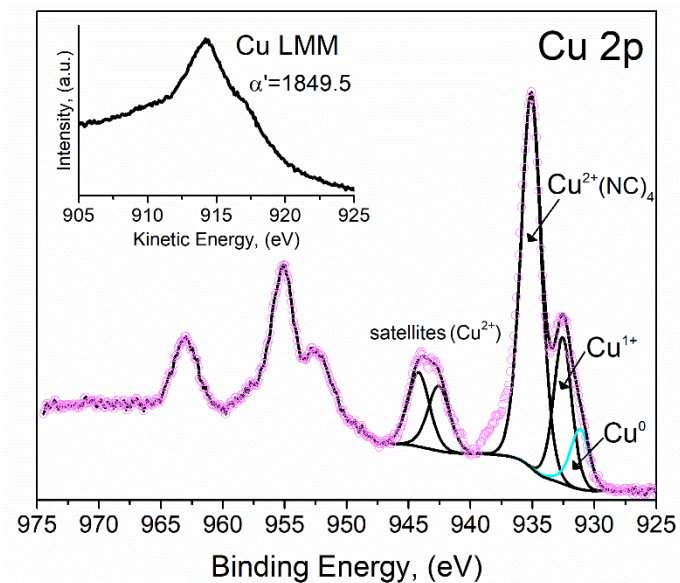
Figure S28: Cu 2p$_{3/2}$ core level peak for Cu(H$_2$O)$_2$[Ni(CN)$_4$]·xH$_2$O with intense satellites. Inset: Cu LMM Auger line. The formation of Cu$^0$ and Cu$^+$ species was observed. According to the binding energy for the Cu$^+$ species, it corresponds to the formation of cuprous cyanide. See Ref. [24] and https://doi.org/10.1016/j.jssc.2019.02.015.
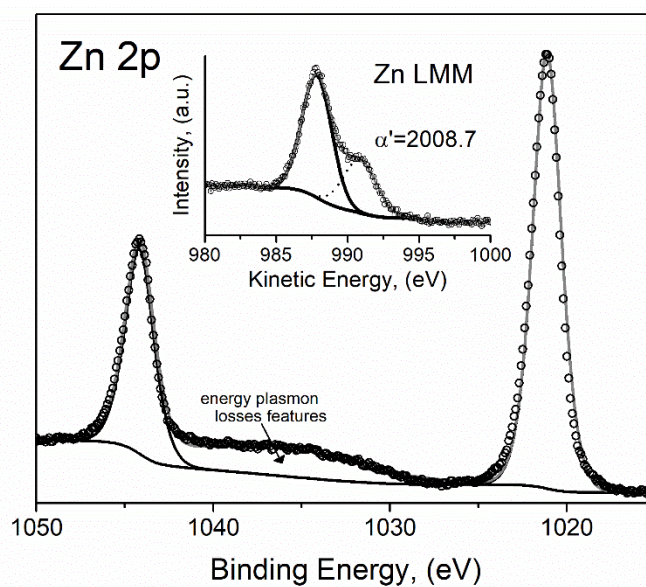


Figure S29: Zn 2p core level peaks for Zn(H$_2$O)$_2$[Ni(CN)$_4$]·xH$_2$O. Inset: The Zn LMM Auger spectral region. The calculated modified Auger parameter ($\alpha'$), 20087, is characteristic of Zn(2+) species.
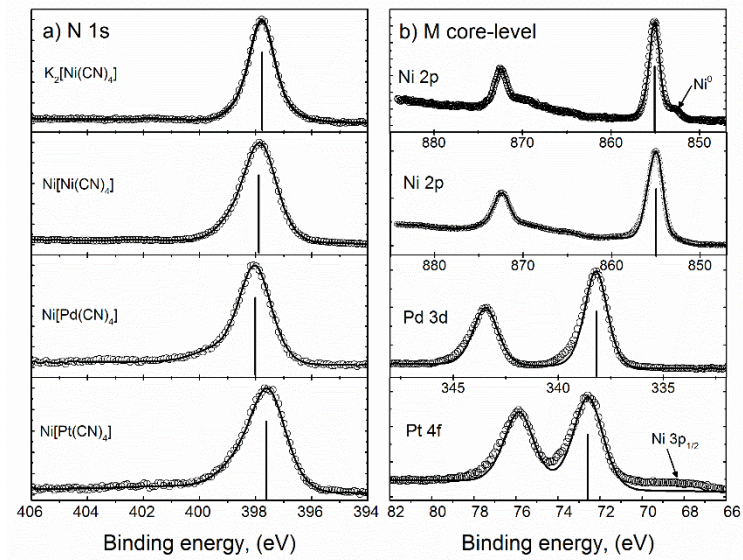
Figure S30. XPS curve fitting for N 1s and M core-levels spectra recorded from Ni[M(CN)$_4$]·uH$_2$O, M = Ni, Pd, Pt series